

Transferable Potentials for Phase Equilibria. 3. Explicit-Hydrogen Description of Normal Alkanes

Bin Chen and J. Ilja Siepmann*

Departments of Chemistry and of Chemical Engineering and Materials Science, University of Minnesota, 207 Pleasant Street SE, Minneapolis, Minnesota 55455-0431

Received: March 9, 1999; In Final Form: April 23, 1999

Motivated by shortcomings of the available united-atom models for alkanes, a new explicit-hydrogen model for *n*-alkanes (TraPPE-EH, transferable potentials for phase equilibria-explicit hydrogen) is developed from fitting to one-component fluid phase properties. In addition to Lennard–Jones sites on carbon atoms, this model utilizes Lennard–Jones sites on the centers of carbon–hydrogen bonds. Configurational-bias Monte Carlo simulations in the Gibbs and canonical ensembles were carried out to calculate the one-component vapor–liquid phase equilibria for methane to *n*-dodecane, to determine the phase diagram of supercritical ethane and *n*-heptane mixtures, to obtain the Gibbs free energies of transfer for *n*-pentane and *n*-hexane between helium vapor and *n*-heptane liquid phases, and to study the high-pressure region of the equation of state for *n*-pentane and *n*-decane. The explicit-hydrogen representation with its more faithful description of the molecular shape of alkanes allows us to find a set of Lennard–Jones parameters that yields significantly better agreement with experiment for one- and multicomponent phase equilibria than our united-atom alkane model, but the price is higher computational cost.

1. Introduction

Sparked by improvements in simulation algorithms and computer power, the prediction of thermophysical properties for systems of technological importance using Monte Carlo and molecular dynamics simulations has become the focus of intense research efforts. Currently, it appears that shortcomings in the available force fields are the main limitation that prevents molecular simulations from making reliable, quantitative predictions of different thermophysical properties over a wide range of physical conditions (temperature and pressure). Because of the technological importance of alkanes for the chemical industries, many research groups have worked on the development of alkane force fields and great strides have been made over the past ten years.^{1–13}

The first two papers in this series^{10,11} were devoted to a force field for linear and branched alkanes (TraPPE-UA, transferable potentials for phase equilibria-united atom) based on the computationally efficient united-atom representation that allows relatively accurate predictions of phase equilibria using only five types of united atoms (methane, methyl, methylene, methine, and quaternary carbon).² However, some problems have been noted for the TraPPE-UA model: (i) it predicts too high saturated vapor densities and pressures, resulting in too low boiling points (while the critical temperature being part of the fitting strategy is correctly reproduced);^{10,11} (ii) standard Gibbs free energies of transfer between helium and liquid alkanes are approximately 1 kJ/mol too high (too small in magnitude);^{14,15} and (iii) close to the triple point, viscosities are too low and diffusion constants are too high.^{16,17} As discussed in the preceding papers in this series, the shortcomings of the TraPPE-UA force field might originate from the use of the united-atom representation, the use of Lennard–Jones potentials for the nonbonded interactions, or the neglect of

many-body interactions.¹⁰ It is known for quite some time that explicit-hydrogen models are more appropriate for simulations of solid or high-density liquid phases.^{18,19} In addition, explicit-hydrogen models allow for the distribution of partial charges on the individual hydrogen and carbon atoms, which may be important to describe the interactions of alkanes with more polar molecules.

As a first step in the investigation of explicit-hydrogen alkane force fields,²⁰ we have recently calculated a set of vapor–liquid coexistence curves for the Williams,¹ OPLS-AA,⁸ and MMFF94⁹ force fields. It was found that the Williams and OPLS-AA force fields yield a better description of the fluid phase equilibria (saturated liquid densities, normal boiling point, and critical point) than many widely used united-atom models (Ryckaert–Bellemans² and OPLS-UA³). However, the agreement with experiment is not fully satisfactory for the Williams and OPLS-AA force fields, and their performance for phase equilibria does not match that of the computationally less demanding TraPPE-UA force field. The MMFF94 alkane force field was found to yield a comparably poor description of the fluid phase equilibria. On the positive side, the investigation of the Williams and OPLS-AA force field showed that these explicit-hydrogen models yield similar relative deviations for the normal boiling and critical temperatures,²⁰ whereas our earlier investigation of three united-atom models showed that the ratios of the simulated over experimental boiling temperature are always smaller than the corresponding ratios for the critical temperatures.¹⁰ Thus, an explicit-hydrogen model with optimized interaction parameters should in principle be able to yield a better description of the fluid phase equilibria than any united-atom force field.

The goal of this work is to derive an explicit-hydrogen force field that overcomes the shortcomings of our TraPPE-UA force field mentioned above. The remainder of this article is arranged as follows. Sections 2 and 3 give descriptions of the novel TraPPE-EH (explicit-hydrogen) force field and the simulation

* Corresponding author: siepmann@chem.umn.edu.

TABLE 1: Bond Lengths, Bond Angles, and Force Constants of the TraPPE-EH Alkane Force Field^a

d_{C-C} [Å]	1.535
d_{C-H} [Å]	1.100
$\theta_0(C-C-C)$ [deg]	112.7
$k_\theta(C-C-C)/k_B$ [K rad ⁻²]	58765
$\theta(C-C-H)$ [deg]	110.7
$\theta(H-C-H)$ [deg]	107.8

^a The bond angle parameters are taken from the OPLS-AA force fields.⁸

details. In the first part of section 4, the performance of the new model for single-component vapor–liquid coexistence curves is discussed. Thereafter, we present simulation results for the high-pressure equation-of-state, for the supercritical ethane/*n*-heptane pressure–composition diagrams at 366 and 450 K, and for the Gibbs free energies of transfer for alkanes between helium and *n*-heptane at standard conditions.

2. The TraPPE-EH Alkane Force Field

A. Bonded Interactions. As in our previous calculations for the fluid phase equilibria of explicit-hydrogen models, we treat the *n*-alkanes as semiflexible chain molecules in a way very similar to the constrained molecular dynamics model used by Ryckaert and co-workers.²⁰ The lengths of all C–C and C–H bonds are fixed, with parameters listed in Table 1. A harmonic bond bending potential is used for all C–C–C bond angles^{8,21}

$$u_{\text{bend}} = \frac{k_\theta}{2} (\theta - \theta_0)^2 \quad (1)$$

where k_θ and θ_0 are the bending force constant and the equilibrium bond angle (the parameters are given in Table 1). The H–C–H bond angles of all units and the C–C–H bond angles containing a methyl group hydrogen are fixed, whereas the C–C–H bond angles, for which the central carbon atom belongs to a methylene segment, are determined via the same geometric construction as used in ref 20. Thus, no contributions to the intramolecular potential energy arise from H–C–H and C–C–H bond angles. The OPLS united-atom torsional potentials³ governs the motion of C–C–C–C dihedral angles

$$u_{\text{tors}}(C-C-C-C) = c_1 [1 + \cos(\phi)] + c_2 [1 - \cos(2\phi)] + c_3 [1 + \cos(3\phi)] \quad (2)$$

with the following numerical constants: $c_1/k_B = 355.03$ K, $c_2/k_B = -68.19$ K, and $c_3/k_B = 791.32$ K. The torsional motion of dihedral angles involving the hydrogen atoms on a methyl group are governed by a threefold symmetric torsional potential

$$u_{\text{tors}}(X-C-C-H) = c_X [1 - \cos(3\phi)] \quad (3)$$

with $c_C/k_B = 854$ K²² and $c_H/k_B = 717$ K.²³ There are no potential energy contributions from torsional angles involving methylene group hydrogens. Nonbonded van der Waals interactions are included for all atoms which are separated by at least three C–C bonds, i.e., there are no 1-4 interactions of any type. The 1-5 interactions involving one hydrogen atom and 1-6 interactions for two hydrogen atoms are also not considered as nonbonded interactions, because they are accounted for by the torsional potentials. The choice of a semiflexible model is computationally very efficient for our Monte Carlo calculations (see section 3). However, it differs from the more flexible models used commonly in biomolecular simulations,²⁴ which treat all bond angles as flexible, explicitly include torsional

potentials for all dihedral angles, and often contain 1-4 nonbonded interactions. Nevertheless, it is believed that the choice of intramolecular potentials is of secondary importance for the determination of thermodynamic properties, such as vapor–liquid phase equilibria, as long as it does not result in a change of the conformational characteristics of the molecule. Thus, if a fully flexible representation of the alkanes is desired, say for molecular dynamics calculations, then we would like to suggest to follow the approach of Tobias and co-workers²⁵ who derived a fully flexible version of the Williams model by combining its nonbonded parameters with bonded parameters from the Smith and Karplus alkane model.²⁶

B. Nonbonded Interactions. All nonbonded interactions are described by pairwise additive Lennard–Jones (LJ) 12-6 potentials

$$u_{\text{LJ}}(r_{ij}) = 4\epsilon_{ij} \left[\left(\frac{\sigma_{ij}}{r_{ij}} \right)^{12} - \left(\frac{\sigma_{ij}}{r_{ij}} \right)^6 \right] \quad (4)$$

where r_{ij} , ϵ_{ij} , and σ_{ij} are the separation, LJ well depth, and LJ size, respectively, for the pair of atoms *i* and *j*. The parameters for unlike interactions are computed using standard Lorentz–Berthelot combining rules:^{27,28}

$$\sigma_{ij} = \frac{1}{2} (\sigma_{ii} + \sigma_{jj}) \quad \epsilon_{ij} = \sqrt{\epsilon_{ii}\epsilon_{jj}} \quad (5)$$

Spherical potential truncations at $r_{\text{cut}} = 9$ Å with analytical tail corrections are used for the Lennard–Jones interactions. Presently, the TraPPE-EH model does not make use of partial charges at the carbon and hydrogen sites. As has already been argued by Jorgensen et al.,²⁹ partial charges (of reasonable magnitude) do not influence the thermodynamic properties of pure liquid alkanes. Similarly, we have found that the partial charges of the OPLS-AA model have no significant influence on the vapor–liquid coexistence curves of linear alkanes.²⁰ In addition, MacKerrell did not observe significant effects of alkane partial charges on alkane free energies of hydration.³⁰

In the TraPPE-EH model, the nonbonded Lennard–Jones interaction sites are located at the carbon atoms and at the centers of carbon–hydrogen bonds. Thus there are no interaction sites at the hydrogen nuclei. The van der Waals interactions arise primarily from the valence electrons,³¹ and a hydrogen atom has only one electron that participates in the formation of the carbon–hydrogen bond. It is well known that the approximation of spherical symmetric interaction potentials is reasonable for larger atoms, while it does not hold for smaller atoms. In the case of the hydrogen atom, centering the Lennard–Jones site at the nucleus is therefore not a good representation, and one should either use anisotropic potentials³¹ or move the center of an isotropic potential along the carbon–hydrogen bond towards the carbon atom. The Williams model¹ is an example where the interaction site is moved inward by about 10% of the bond length, and this displacement improves the prediction of the crystal packing of hydrocarbons.^{32,33} Other force fields have adopted similar displacements.^{34–36} For the TraPPE-EH model, we selected a more dramatic change by placing the interaction site at the center of the carbon–hydrogen bond where the electron density is largest, similar to the method of bond–bond interaction used by Salem and Amos.^{37–40} Short test simulations proved that this large displacement yields better results than a displacement by 10% as used in the Williams model. To some extent, one might also argue that an additional interaction site should be placed at the center of carbon–carbon bonds to mimic the interaction of the valence electrons involved in the formation

TABLE 2: Lennard–Jones Parameters of the TraPPE-EH Alkane Force Field

	contribution to the site	ϵ/k_B [K]	σ [Å]
C–H	(Csp ³ , H1s) σ bond	15.3	3.31
methane carbon	(C1s ²) core	0.01	3.31
methyl carbon	(C1s ²) core + 1/2 (Csp ³ , Csp ³) σ bond	4.0	3.30
methylene carbon	(C1s ²) core + 2 \times 1/2 (Csp ³ , Csp ³) σ bond	5.0	3.65

^a The C–H site is placed at the center of any carbon–hydrogen bond.

of that bond. However, this would lead to a further increase in the total number of interaction sites for a given alkane. Thus we decided to account for the interactions of the carbon core electrons and of those carbon valence electrons involved in carbon–carbon bonds by isotropic Lennard–Jones potentials centered at the carbon atoms. This will require different Lennard–Jones parameters for the carbon atom in methane, methyl, and methylene groups because of their different numbers of carbon–carbon bonds (see also Table 2). Nevertheless, besides avoiding an increase in the number of interactions sites, there are two further arguments that justify neglecting an additional site centered on the carbon–carbon bonds. First, the contribution to the molecular polarizability from the carbon–carbon bond is small. This is evident from the TraPPE-UA force field¹⁰ where the ϵ parameters are found to be proportional to the square of the number of the carbon–hydrogen bonds contained in the pseudoatoms, or, in other words, the polarizability of these pseudoatoms is proportional to the number of the carbon–hydrogen bonds. Second, the carbon–carbon bond is inside the surrounding carbon and carbon–hydrogen interaction sites and thus does not influence the overall shape of the molecule, whereas displacement of the carbon–hydrogen interaction sites towards the carbon atoms is required to represent the nonspherical electron density around the hydrogen atoms.

The following fitting strategy is employed in this work. First, the parameters for the interaction site on the carbon–hydrogen bond are determined by fitting to the vapor–liquid coexistence curve of methane. All four carbon valence electrons take part in the formation of the carbon–hydrogen bonds, and the polarizability on the carbon arising from the 1s core electrons is believed to be *very* small.^{37–40} Since it is not possible to fit the methane carbon parameters independently from the parameters of the carbon–hydrogen bonds, we gave the methane carbon atom the following ad hoc parameters: $\sigma(\text{C}_{\text{methane}}) = 3.31$ Å and $\epsilon(\text{C}_{\text{methane}})/k_B = 0.01$ K (where k_B is Boltzmann’s constant). Once the parameters for the carbon–hydrogen bond are established, these remain the same for all other alkanes, and the parameters for the methyl carbon can be obtained from simulations for ethane which consists of two methyl carbons and six carbon–hydrogen bonds in the TraPPE-EH representation. Thereafter, the parameters for the methylene carbon were determined by fitting to *n*-pentane using the previously obtained parameters for the twelve carbon–hydrogen bonds and two methyl carbons. The final set of the TraPPE-EH Lennard–Jones parameters is listed in Table 2. Here we should emphasize that these TraPPE-EH parameters are effective parameters that account to some extent for many-body effects, because of the fitting to vapor–liquid coexistence curves. Furthermore, using the same set of parameters (say, carbon–hydrogen bond parameters) for all alkanes is an approximation that assumes that neighboring groups have only a negligible influence on the polarizability of a given site. Finally, it is important to keep in mind that a carbon–hydrogen bond site accounts for the

polarizability of two valence electrons in the C–H σ bond and that the carbon sites mainly account for the carbon core electrons and the C–C σ bonds. Thus these sites should not be confused with the hydrogen and carbon sites used in standard molecular mechanics force fields.

III. Computational Details

A. Vapor–Liquid Coexistence Curves. A combination of the Gibbs Ensemble Monte Carlo method (GEMC)^{41–43} and the configurational-bias Monte Carlo (CBMC) algorithm^{44–48} was employed to study the vapor–liquid phase equilibria for six linear alkanes. The system sizes (number of alkane molecules and combined volume of the two simulation boxes) were chosen to yield liquid phase simulation boxes with linear dimensions of at least 20 Å and larger vapor phases containing at least 10 molecules. A total of 300 methane, 240 ethane, 180 *n*-propane, 120 *n*-pentane, 90 *n*-octane, or 120 *n*-dodecane molecules were used in these simulations. Further details of the Gibbs ensemble simulations can be found in ref 20. All simulation runs were equilibrated for at least 10 000 Monte Carlo cycles, and the production periods consisted of 50 000 Monte Carlo cycles. The statistical uncertainties in the saturated densities and vapor pressures were estimated by dividing the simulations into 10 blocks.

B. Second Virial Coefficients. The second virial coefficient, $B(T)$, is given by^{49,50}

$$B(T) = -2\pi \int [\langle \exp[-U_{\text{inter}}(r_{12})/k_B T] \rangle_{\alpha_1, \alpha_2} - 1] r_{12}^2 dr_{12} \quad (6)$$

where $U_{\text{inter}}(r_{12})$ is the intermolecular dimer energy when the distance between the COM of molecules 1 and 2 is r_{12} , and $\langle \dots \rangle_{\alpha_1, \alpha_2}$ denotes the canonical ensemble average sampled over conformations of molecules 1 and 2, which are Boltzmann weighted solely on their intramolecular energies by utilizing two simulation boxes.¹⁰ 5000 conformations were utilized to calculate the ensemble average, and the integral was evaluated from 0 to 500 Å with a 0.05 Å step size.

C. High-Pressure Equation of State. Simulations in the canonical ensemble were performed to study the high-pressure *pVT* behavior of *n*-pentane and *n*-decane. The MC moves were equally divided between CBMC, translation, and rotation. The simulations were carried out for 120 *n*-pentane and *n*-decane molecules. For *n*-pentane, one additional simulation was carried out for 512 molecules to investigate the system-size effects. At least 10 000 MC cycles were used for equilibration and production.

D. Supercritical Pressure–Composition Diagram of Ethane and *n*-Heptane. Simulations for the binary system were carried out using the isobaric version of the Gibbs ensemble⁴² combined with the CBMC technique. The 366 and 450 K isotherms were obtained for the supercritical pressure–composition diagram of ethane and *n*-heptane. A total number of 400 molecules was used. For both isotherms, simulations of the mixture were carried out for at least four different external pressures. In addition, *NVT* Gibbs ensemble simulations for pure *n*-heptane (120 molecules) were performed at 366 and 450 K to calculate the corresponding saturated vapor pressures. The production run consisted of 100 000 Monte Carlo cycles.

E. Helium to *n*-Heptane Gibbs Free Energies of Transfer. Simulations for the multicomponent systems (helium, *n*-heptane, plus solute molecules) were carried out in the *NpT* Gibbs ensemble at $T = 298$ K and $p = 101.3$ kPa. Three independent simulations were performed: (run A) using 2 *n*-pentane solutes, (run B) using 2 *n*-hexane solutes, and (run C) using 2 *n*-pentane

TABLE 3: Numerical Results of the Gibbs-Ensemble Simulations for *n*-Alkanes Using the TraPPE-EH Force Field^a

<i>T</i>	<i>p</i>	ρ_{vap}	ρ_{liq}
methane			
105	0.066 ₁	0.00124 ₃	0.4375 ₄
120	0.206 ₇	0.0035 ₁	0.4142 ₅
135	0.501 ₁₅	0.0079 ₂	0.388 ₁
150	1.161 ₃₈	0.018 ₁	0.361 ₁
165	2.04 ₆	0.032 ₁	0.323 ₂
175	2.89 ₉	0.048 ₂	0.296 ₃
propane			
240	0.146 ₈	0.0034 ₂	0.564 ₁
260	0.302 ₁₁	0.0066 ₃	0.539 ₁
280	0.582 ₂₃	0.0124 ₅	0.513 ₂
300	0.973 ₄₃	0.021 ₁	0.481 ₂
320	1.641 ₅₅	0.035 ₂	0.453 ₂
340	2.62 ₁₄	0.066 ₈	0.411 ₆
<i>n</i> -octane			
400	0.105 ₈	0.0038 ₃	0.608 ₂
440	0.306 ₁₂	0.0107 ₅	0.573 ₁
470	0.521 ₂₂	0.018 ₁	0.531 ₂
500	0.909 ₃₈	0.032 ₂	0.502 ₄
530	1.424 ₃₂	0.053 ₃	0.452 ₄
550	1.93 ₁₁	0.076 ₁₀	0.402 ₁₃
ethane			
185	0.101 ₃	0.0020 ₁	0.536 ₁
215	0.447 ₁₃	0.0083 ₃	0.498 ₁
230	0.688 ₃₁	0.0122 ₆	0.475 ₁
245	1.140 ₆₁	0.020 ₁	0.452 ₂
260	1.75 ₁₂	0.031 ₃	0.428 ₂
275	2.65 ₁₄	0.052 ₄	0.395 ₅
<i>n</i> -pentane			
330	0.209 ₅	0.0059 ₁	0.585 ₁
360	0.461 ₃₆	0.013 ₁	0.550 ₁
390	0.864 ₄₆	0.023 ₁	0.510 ₁
420	1.565 ₈₇	0.044 ₄	0.464 ₇
440	2.23 ₁₃	0.068 ₈	0.429 ₅
450	2.93 ₈	0.102 ₁₀	0.407 ₂₁
<i>n</i> -dodecane			
450	0.035 ₂	0.0016 ₁	0.630 ₁
500	0.111 ₆	0.0048 ₃	0.581 ₂
550	0.310 ₁₄	0.0128 ₅	0.533 ₁
585	0.629 ₃₀	0.027 ₁	0.483 ₄
620	1.154 ₇₃	0.056 ₅	0.449 ₄

^a Temperatures, (vapor) pressures, and orthobaric densities are given in units of K, MPa, and g/mL, respectively. The subscripts give the statistical accuracies of the last decimal(s).

and 2 *n*-hexane solutes. In each case the system contained 210 helium and 140 *n*-heptane molecules. The systems were equilibrated for 30 000 MC cycles, and the production periods consisted of 360 000 MC cycles.

IV. Results and Discussion

A. Vapor–Liquid Coexistence Curves. The vapor–liquid coexistence curves were calculated for six linear alkanes (methane, ethane, propane, pentane, octane, and dodecane) using the TraPPE-EH force field (see Figure 1 and Table 3). The corresponding critical data and normal boiling points together with simulation results for the OPLS-UA, OPLS-AA, and TraPPE-UA force fields are summarized in Table 4. Agreement for the TraPPE-EH force field with the experimental data^{51,52} is very satisfactory: critical temperatures and normal boiling points deviate by less than 1% (with the exception of T_c for *n*-dodecane); the saturated liquid densities deviate by less than 2%, while the saturated gas densities show slightly larger deviations (but have also larger relative statistical uncertainties).

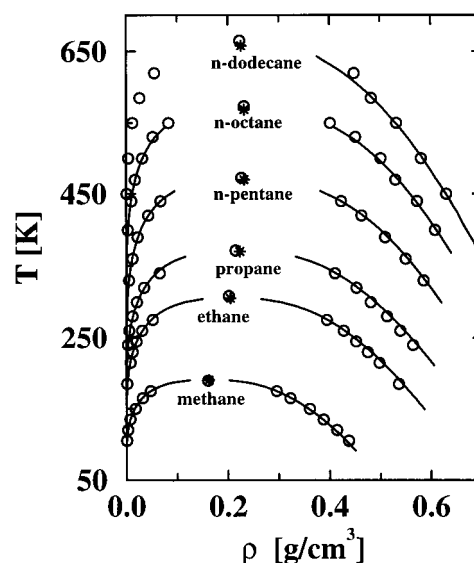


Figure 1. Vapor–liquid coexistence curves for methane, ethane, propane, *n*-pentane, *n*-octane, and *n*-dodecane. Calculated coexistence densities and extrapolated critical points for the TraPPE-EH model are shown as open circles. Experimental coexistence data and critical points are shown as solid lines and stars.^{51,52}

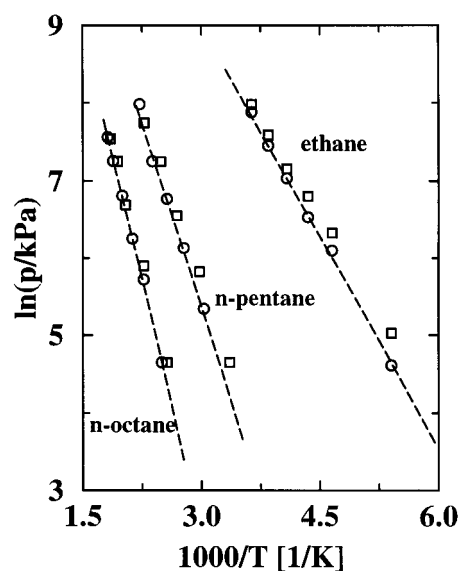


Figure 2. Clausius–Clapeyron plots of the saturated vapor pressure against the inverse temperature for ethane, *n*-pentane, and *n*-octane for the TraPPE-UA (open squares) and TraPPE-EH (open circles) force fields.¹⁰ Dashed lines represent the experimental data.⁵²

The performance of the TraPPE-EH force field in reproducing the experimental critical data and saturated liquid densities is at least as good as that of the TraPPE-UA force field. However, as is evident from Clausius–Clapeyron plots (see Figure 2), the TraPPE-EH force field provides great improvements on the vapor side of the fluid phase diagram yielding much better results for saturated vapor densities and pressures and, correspondingly, normal boiling points. The differences between TraPPE-EH and TraPPE-UA force fields are more apparent when the coexistence curves are shown as functions of molar volume (see Figure 3). In particular, at low temperatures the TraPPE-UA model tends to greatly underestimate the saturated vapor molar volumes. Whereas there appears to be no significant difference between the TraPPE-UA and TraPPE-EH models for the saturated molar volumes (or specific densities) of the liquid phases.

TABLE 4: Thermodynamic Properties of *n*-Alkanes Calculated for the OPLS-UA,^{3,10} OPLS-AA,^{8,20} TraPPE-UA,¹⁰ and TraPPE-EH Force Fields^a

<i>n</i> -alkane	property	OPLS-UA	OPLS-AA	TraPPE-EH	TraPPE-UA	exp
methane	T_b (K)	112 ₁	114 ₁	110.3 ₃	112 ₁	111.6
	T_c (K)	191 ₁	191 ₂	189.6 ₆	191 ₁	190.6
	ρ_c (g/mL)	0.160 ₃	0.170 ₆	0.161 ₁	0.160 ₃	0.162
	p_c (MPa)	4.5 ₁₁	4.6 ₉	4.5 ₃	4.5 ₁₁	4.6
	f_{acc}	-0.020	0.070	0.016	-0.020	0.0108
ethane	T_b (K)	190 ₁	178 ₂	185 ₁	177 ₁	185
	T_c (K)	323 ₂	285 ₂	308 ₂	304 ₂	305
	ρ_c (g/mL)	0.206 ₃	0.202 ₇	0.202 ₃	0.206 ₃	0.205
	p_c (MPa)	5.1 ₄	4.7 ₁₃	5.3 ₇	5.1 ₄	4.9
	f_{acc}	0.071	0.164	0.101	0.016	0.099
propane	T_b (K)			232 ₁		231
	T_c (K)			372 ₂		370
	ρ_c (g/mL)			0.215 ₃		0.223
	p_c (MPa)			4.6 ₃		4.3
	f_{acc}			0.173		0.152
<i>n</i> -pentane	T_b (K)	327 ₃	301 ₄	311 ₃	296 ₂	309
	T_c (K)	517 ₅	458 ₅	473 ₃	470 ₂	470
	ρ_c (g/mL)	0.226 ₇	0.225 ₁₄	0.227 ₄	0.238 ₄	0.232
	p_c (MPa)	3.6 ₁₃	3.3 ₁₃	3.6 ₂	3.7 ₁	3.4
	f_{acc}	0.145	0.238	0.224	0.140	0.249
<i>n</i> -octane	T_b (K)	442 ₄	394 ₅	398 ₂	386 ₂	399
	T_c (K)	656 ₅	558 ₈	574 ₃	570 ₂	569
	ρ_c (g/mL)	0.235 ₉	0.233 ₁₆	0.232 ₃	0.239 ₂	0.232
	p_c (MPa)	2.8 ₂₃	2.9 ₁₇	2.6 ₃	2.6 ₁	2.5
	f_{acc}	0.326	0.486	0.442	0.319	0.394
<i>n</i> -dodecane	T_b (K)			494 ₂	480 ₂	489
	T_c (K)			667 ₂	667 ₅	658
	ρ_c (g/mL)			0.223 ₂	0.235 ₆	0.226
	p_c (MPa)			2.0 ₄	2.3 ₂	1.8
	f_{acc}			0.583	0.495	0.577

^a T_b , T_c , ρ_c , p_c , f_{acc} are the normal boiling point, the critical temperature, the critical density, the critical pressure, and the accentric factor, respectively. The experimental data are taken from refs 52 and 62. The subscripts give the statistical accuracies of the last decimal(s).

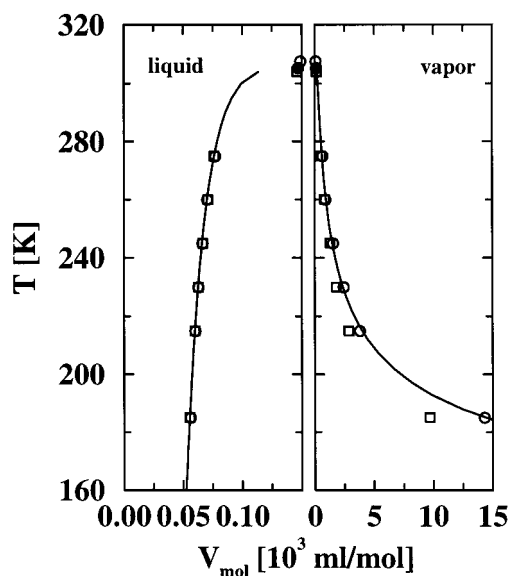


Figure 3. Comparison of the saturated molar volumes for ethane calculated using the TraPPE-UA (open squares) and TraPPE-EH (open circles) force fields. Solid lines and filled circles represent the experimental data.^{51,52}

Following from the results for single-component phase equilibria, it is clear that the TraPPE-EH force field gives a better representation of the *n*-alkanes than does the TraPPE-UA force field. Can this observation be generalized to other united-atom and explicit-hydrogen models? The ratios of the calculated over the experimental T_b and T_c are compared in Figure 4 for the OPLS and TraPPE force fields. The two united-atom versions consistently give a lower ratio for T_b than for T_c , or in other words, their accentric factors are too low. The

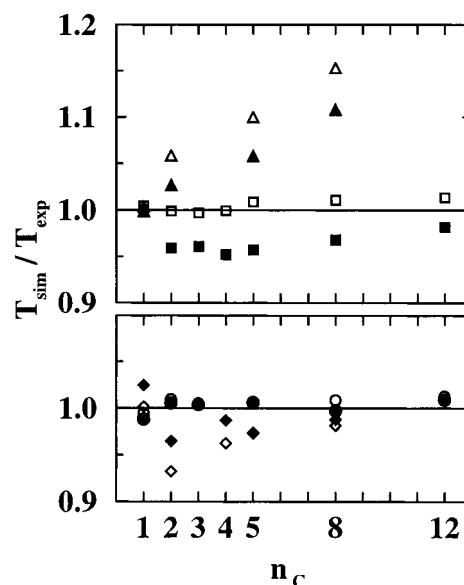


Figure 4. Ratios of calculated to experimental^{51,52} critical temperatures (open symbols) and normal boiling points (filled symbols) versus the chain length for the OPLS-UA (triangles),³ OPLS-AA (diamonds),⁸ TraPPE-UA (squares),¹⁰ and TraPPE-EH (circles) force fields.

TraPPE-EH force field yields values close to unity for T_b and T_c . (Not shown are results for the Williams force field¹ that also gives similar ratios for T_b and T_c , but both ratios are significantly too low.²⁰) The pattern is reversed for the OPLS-AA force field⁸ which produces larger ratios for T_b than for T_c .²⁰ The corresponding accentric factors are listed in Table 4. This comparison lets us conclude that a good representation of the shape of a molecule is essential for the performance of a force field. Tildesley and co-workers⁵³ have calculated the

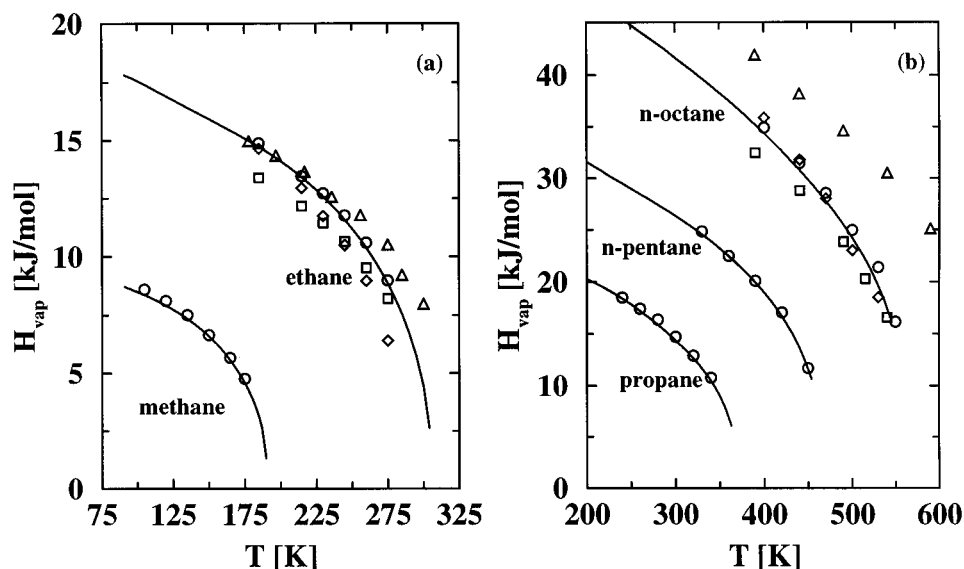


Figure 5. Heats of vaporization for methane, ethane (part a), propane, *n*-pentane, and *n*-octane (part b) calculated for the TraPPE-EH (open circles) force field. The results for ethane and *n*-octane using the OPLS-UA (open triangles),^{3,10} OPLS-AA (open diamonds),^{8,20} and TraPPE-UA (open squares)¹⁰ force fields are also plotted for comparison. The solid lines represent the experimental data.⁵²

TABLE 5: Comparison of the Individual Energetic and pV Terms for the Vapor and Liquid Phases of Ethane between the TraPPE-UA¹⁰ and TraPPE-EH Force Fields^a

T	$E_{\text{tot,liq}}$	$E_{\text{tot,vap}}$	$E_{\text{int,liq}}$	$E_{\text{int,vap}}$	$E_{\text{tors,liq}}$	$E_{\text{tors,vap}}$	$\Delta(pV)$	ΔH_{vap}	$\Delta H_{\text{vap,exp}}$
TraPPE-EH									
185	-13.05 ₅	0.35 ₁	-13.52 ₅	-0.09 ₁	0.42 ₁	0.43 ₁	1.54 ₂	14.90 ₄	14.73
215	-11.66 ₉	0.19 ₃	-12.12 ₉	-0.29 ₂	0.46 ₁	0.48 ₁	1.62 ₂	13.47 ₁₀	13.41
230	-11.00 ₈	0.08 ₂	-11.50 ₈	-0.42 ₂	0.50 ₁	0.51 ₁	1.65 ₂	12.73 ₈	12.58
245	-10.36 ₈	-0.14 ₃	-10.90 ₆	-0.66 ₃	0.54 ₂	0.52 ₄	1.55 ₂	11.77 ₅	11.59
260	-9.64 ₆	-0.46 ₁₀	-10.22 ₆	-1.01 ₁₀	0.58 ₂	0.57 ₃	1.42 ₃	10.60 ₁₃	10.38
275	-8.44 ₂₅	-0.87 ₁₅	-9.04 ₂₀	-1.45 ₁₅	0.60 ₁	0.58 ₁	1.43 ₅	9.00 ₃₈	8.86
TraPPE-UA									
185	-12.04 ₈	-0.11 ₁	-12.04 ₈	-0.11 ₁			1.47 ₂	13.40 ₅	
215	-10.93 ₁₁	-0.34 ₁	-10.93 ₁₁	-0.34 ₁			1.58 ₂	12.17 ₁₀	
230	-10.35 ₃	-0.50 ₂	-10.35 ₃	-0.50 ₂			1.60 ₂	11.45 ₈	
245	-9.71 ₈	-0.66 ₃	-9.71 ₆	-0.66 ₃			1.55 ₂	10.65 ₁₀	
260	-9.04 ₂	-1.02 ₁	-9.04 ₂	-1.02 ₁			1.50 ₃	9.52 ₅	
275	-8.34 ₁₂	-1.49 ₂₂	-8.34 ₁₂	-1.49 ₂₂			1.35 ₆	8.20 ₃₀	

^a Temperatures and all individual energetic and pV terms are in units of K and kJ/mol, respectively. $E_{\text{tot,liq}}$, $E_{\text{tot,vap}}$, $E_{\text{int,liq}}$, $E_{\text{int,vap}}$, $E_{\text{tors,liq}}$, and $E_{\text{tors,vap}}$ are the total liquid energy, the total vapor energy, the intermolecular liquid energy, the intermolecular vapor energy, the liquid torsional energy, and the vapor torsional energy, respectively. Experimental heats of vaporization are taken from ref 52. Subscripts give the statistical accuracies of the last decimal(s).

vapor–liquid phase diagrams of Lennard–Jones dimers for a set of different bond lengths and found that changing the ratio between bead size and bond length alters the shape and accentric factor for the phase diagrams. We have performed some additional calculations for Lennard–Jones dimers varying the reduced bond length over a larger range and observed a considerable increase of the ratio of T_b over T_c for increasing bond length ranging from $T_b/T_c = 0.57$ for $l/\sigma = 0$ to $T_b/T_c = 0.76$ for $l/\sigma = 5$ (the boiling point is calculated at $p = 0.00734$ in reduced unit).⁵⁴ The TraPPE-UA force field may be viewed as an explicit-hydrogen model with zero bond length. Comparing the TraPPE-UA, TraPPE-EH, and OPLS-AA models, it can be observed that there is an increase in the well depth of the carbon–hydrogen or hydrogen interaction site and that it moves from the carbon position, to the center of the carbon–hydrogen bond, and to the position of the hydrogen nucleus. Concurrently, the accentric factors are too low for the TraPPE-UA force field, in good agreement for the TraPPE-EH force field, and too high for the OPLS-AA model.

A similar pattern can be extracted from comparison of heats of vaporization as functions of temperature which are shown

in Figure 5. The TraPPE-EH force field yields good agreement with experiment for all linear alkanes over the entire range of temperatures studied. Whereas the TraPPE-UA model yields heats of vaporization that are 1 to 2 kJ/mol too low at the normal boiling point, better results at higher temperatures should be expected from a model that has been fitted to the critical temperatures. In contrast, the OPLS-AA force field predicts satisfactory heats of vaporization near the normal boiling points (which were part of the fitting procedure), but too low values at the higher temperatures. Table 5 and Figure 6 compare the individual energetic and pV terms for ethane for the vapor and liquid phase between the TraPPE-UA and TraPPE-EH force field. First, the torsional energies⁵⁵ (only present for TraPPE-EH) are very similar for the coexisting vapor and liquid phases. Thus, only the intermolecular Lennard–Jones terms contribute significantly to the change in internal energy upon transfer from liquid to vapor phase. Furthermore, the vapor phase energies and pV terms are very similar for both force fields. Thus, we have to conclude that differences in the intermolecular Lennard–Jones energies of the liquid phases are solely responsible for the differences between the TraPPE-UA and TraPPE-EH

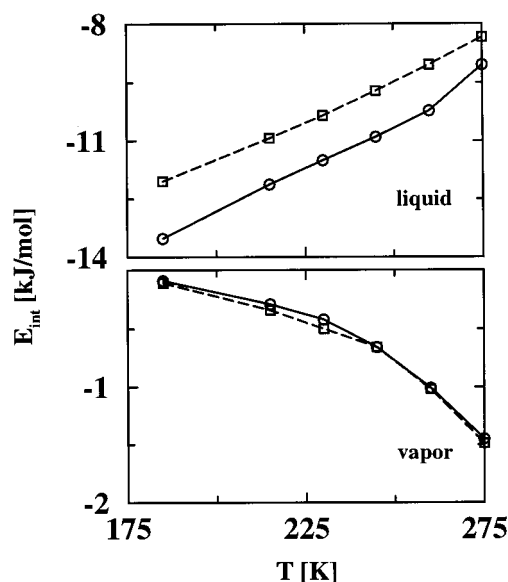


Figure 6. Calculated vapor and liquid phase intermolecular energy for ethane versus temperature for the TraPPE-UA (dashed lines and open squares) and TraPPE-EH (solid lines and open circles) force fields.

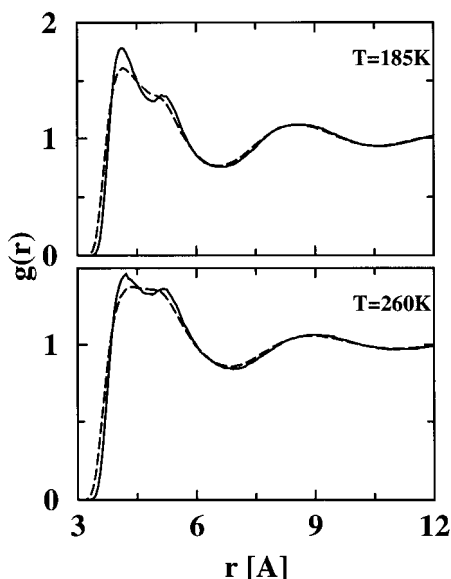


Figure 7. Comparison of carbon-carbon radial distribution functions of liquid ethane at 185 and 260 K for the TraPPE-UA (dashed lines) and TraPPE-EH (solid lines) force fields.

models. Are these differences in intermolecular Lennard-Jones energies coupled to significant changes in the structures of the liquid phases? Carbon-carbon radial distribution functions for ethane and *n*-heptane at two different temperatures are compared in Figures 7 and 8. For ethane, the liquid phases found for the TraPPE-EH force field are slightly more structured in the first solvation shell ($3.5 \text{ \AA} < r < 5.5 \text{ \AA}$). For *n*-heptane, both force fields produce different radial distribution functions for the three types of carbon-carbon pairs, but the agreement between united-atom and explicit-hydrogen representations is very good. The differences between the two force fields are certainly not striking, and we have to conclude that it is the packing of the hydrogen sites that leads to the differences between the two force fields.

B. Second Virial Coefficients. The second virial coefficients for the TraPPE-EH and TraPPE-UA force fields are listed in Table 6. Both models yield second virial coefficients that are consistently smaller in magnitude than the experimental re-

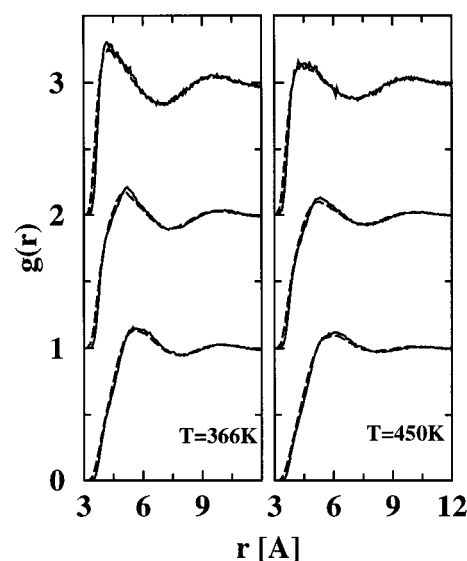


Figure 8. Comparison of carbon-carbon radial distribution functions of liquid *n*-heptane at 366 and 450 K for the TraPPE-UA (dashed lines) and TraPPE-EH (solid lines) force fields. The data for methyl carbon-methyl carbon pairs and methyl carbon-methylene carbon pairs are displaced vertically by 2 and 1 unit(s), respectively.

TABLE 6: Comparison of the Second Virial Coefficients Calculated for *n*-Alkanes Using the TraPPE-UA¹⁰ and TraPPE-EH Models^a

<i>n</i> -alkane	<i>T</i> [K]	TraPPE-UA	TraPPE-EH	exp
ethane	298.2	-159 ₁	-172 ₁	-185
	348.2	-115 ₁	-123 ₁	-135
	423.2	-73 ₁	-77 ₁	-88
<i>n</i> -pentane	173	-3841 ₁₃₉	-4991 ₉₄	-13005
	247	-1407 ₁₄	-1657 ₂₁	-2232
	321	-791 ₁₆	-876 ₁₀	-1003
<i>n</i> -hexane	395	-496 ₆	-538 ₄	-602
	207	-3838 ₈₀	-4867 ₂₀₁	-9573
	304	-1338 ₂₁	-1547 ₂₇	-1845
<i>n</i> -octane	425	-628 ₁₃	-685 ₁₃	-745
	288	-3234 ₅₂	-4138 ₁₁₅	-5278
	368	-1685 ₄₂	-1887 ₂₉	-2179
	448	-1018 ₇	-1126 ₁₁	-1245
	528	-676 ₃₁	-737 ₃₀	-810

^a The experimental data are taken from Dymond and Smith⁵⁶ for ethane and from Smith and Srivastava⁵² for the other alkanes. The unit for the second virial coefficient is mL/mol. Subscripts give the statistical accuracies of the last decimal(s).

sults.^{52,56} Deviations of approximately 10% should be expected at high temperatures because the TraPPE force fields are effective force fields that do not explicitly account for many-body dispersive interactions and their nonbonded interactions parameters are derived by fitting to condensed phase properties. The TraPPE-EH force field shows slightly better agreement with experiment.

C. High-Pressure Equation of State. The pressures for high-density "isochores" (the volumes of the experimental cells are not constant over this pressure range^{57,58}) of *n*-pentane and *n*-decane have been computed for the TraPPE-UA and TraPPE-EH force fields (see Table 7). The result given by the simulation for 512 *n*-pentane molecules at 313.15 K is $86 \pm 2 \text{ MPa}$, which agrees well with $89 \pm 2 \text{ MPa}$ for 120 *n*-pentane molecules. Neither the TraPPE-UA nor TraPPE-EH force field is able to yield satisfactory results for both chain lengths, whereas Toxvaerd's anisotropic united-atom force field excels in this respect.^{4,59} While agreement with the experimental results is acceptable for *n*-decane, the pressures for *n*-pentane are too high for the TraPPE-EH force field. On the contrary, the TraPPE-

TABLE 7: Pressure versus Temperature Data Computed from Canonical Simulations for “Isochores” of *n*-Pentane and *n*-Decane using the TraPPE-UA¹⁰ and TraPPE-EH Models^a

<i>n</i> -alkane	<i>T</i> [K]	ρ_{exp} [g/mL]	p_{exp} [MPa]	p_{UA} [MPa]	p_{EH} [MPa]
<i>n</i> -pentane	313.15	0.673	60.5	60.0 ₆	88.5 ₁₇
	443.15	0.666	160.1	154.2 ₁₁	204.9 ₁₄
	543.15	0.661	225.3	215.5 ₇	280.7 ₂₁
<i>n</i> -decane	313.15	0.741	35.7	21 ₂	38.0 ₁₅
	453.15	0.733	153.1	117 ₄	159.1 ₁₂
	553.15	0.728	224.7	175 ₃	232.3 ₁₅

^a Experimental pressures are shown along with the recommended corrected densities.^{57,58} Subscripts give the statistical accuracies of the last decimal(s).

UA force field performs better for *n*-pentane than for *n*-decane. Obviously, the fitting strategy used for the TraPPE force fields does not ensure quantitative *pVT* data at high pressures.

D. Supercritical Pressure–Composition Diagram of Ethane and *n*-Heptane. The 366 and 450 K isotherms for the binary mixture of supercritical ethane and *n*-heptane calculated for the TraPPE-EH, TraPPE-UA, and OPLS-AA force fields are presented in Figure 9 and Table 8. At 366 K, the TraPPE-UA and TraPPE-EH models yield quantitative agreement with experiment.⁶⁰ The only minor difference is that the TraPPE-EH force field predicts slightly lower mole fractions of *n*-heptane in the supercritical phase. In contrast, the performance of the

OPLS-AA model, in particular for the liquid *n*-heptane phase, is not satisfactory. The low solubility of ethane in *n*-heptane observed for the OPLS-AA can be attributed to the too low critical temperature of pure ethane. Obviously small deviations in single-component phase diagrams lead to larger deviations for multicomponent systems. At 450 K, only the TraPPE-EH force field gives good agreement with the experimental data, while there is a larger deviation in the composition of the supercritical phase for the TraPPE-UA model. However, it should be emphasized that the relative deviations in the mole fractions of *n*-heptane in the supercritical phase are similar for both temperatures for the TraPPE-UA model. NVT Gibbs ensemble simulations of pure *n*-heptane were performed at 366 and 450 K (see Table 9). As discussed above, the vapor pressures given by the TraPPE-UA model were too high and the heats of vaporization were too low. While the TraPPE-EH model predicted the best results. The OPLS-AA model, however, yields a good vapor pressure at 366 K, but too high vapor pressure at 450 K.

E. Helium to *n*-Heptane Gibbs Free Energies of Transfer.

The Gibbs free energies of transfer for *n*-pentane, *n*-hexane, and *n*-heptane at *T* = 298 K and *p* = 101.3 kPa were calculated using three different set-ups for the TraPPE-EH force field (see section III.E). The free energies are listed in Table 10, and it is evident that the three independent runs yield results that agree to within the statistical precision of the calculations. The free

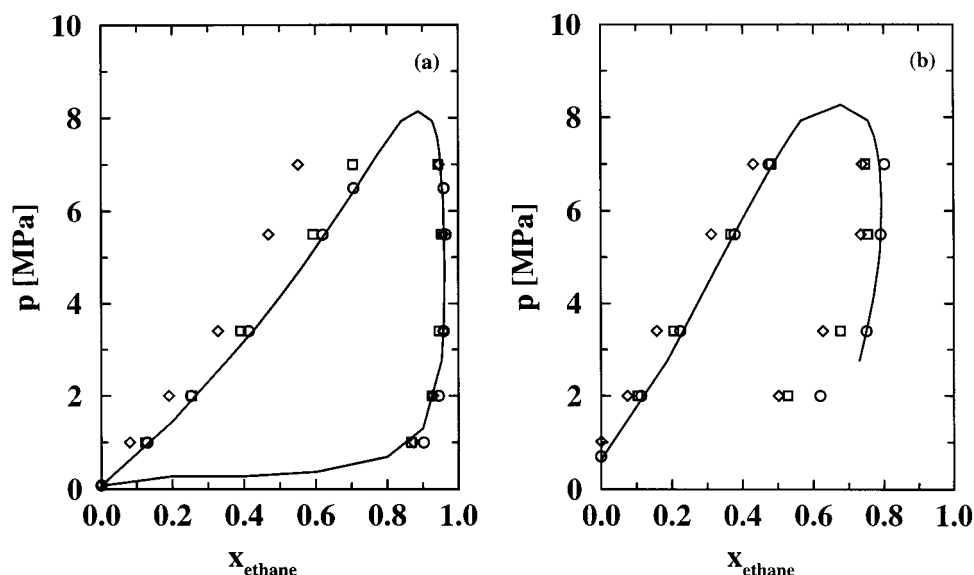


Figure 9. (a) Pressure–composition diagram for the 366 K isotherm of the binary mixture consisting of supercritical ethane and *n*-heptane calculated using the OPLS-AA (open diamonds),⁸ TraPPE-UA (open squares),¹⁰ and TraPPE-EH (open circles) force fields. The solid line represents the experimental results.⁶⁰ (b) The 450 K isotherm for the binary mixture of supercritical ethane and *n*-heptane. Symbols as in Figure 9a.

TABLE 8: Compositions and Densities for the Supercritical Ethane and *n*-Heptane Mixtures at 366 and 450 K Using the OPLS-AA⁸ and TraPPE-EH Force Fields^a

<i>T</i> [K]	<i>p</i> [MPa]	OPLS-AA				TraPPE-EH			
		<i>x</i> _{vap}	<i>x</i> _{liq}	ρ_{vap} [g/mL]	ρ_{liq} [g/mL]	<i>x</i> _{vap}	<i>x</i> _{liq}	ρ_{vap} [g/mL]	ρ_{liq} [g/mL]
366	1.0	0.081 ₁₂	0.875 ₁₆	0.013 ₁	0.607 ₄	0.130 ₆	0.902 ₄	0.0129 ₂	0.599 ₃
	2.0	0.191 ₁₇	0.929 ₁₀	0.0249 ₁	0.594 ₄	0.252 ₁₈	0.946 ₄	0.0245 ₄	0.579 ₅
	3.4	0.328 ₁₉	0.958 ₆	0.044 ₃	0.573 ₁₁	0.414 ₃₁	0.960 ₈	0.044 ₁	0.547 ₁₂
	5.5	0.469 ₁₉	0.958 ₁₀	0.075 ₄	0.523 ₁₁	0.621 ₂₁	0.965 ₄	0.082 ₃	0.485 ₂₀
	6.5					0.707 ₄₁	0.960 ₁₅	0.082 ₃	0.485 ₂₀
	7.0	0.551 ₂₂	0.946 ₇	0.109 ₇	0.500 ₁₃				
450	2.0	0.075 ₁₀	0.502 ₁₉	0.042 ₂	0.505 ₁₁	0.114 ₁₀	0.620 ₂	0.036 ₂	0.507 ₇
	3.4	0.158 ₁₀	0.627 ₂₅	0.063 ₄	0.490 ₆	0.225 ₁₀	0.750 ₁₉	0.053 ₃	0.487 ₁₁
	5.5	0.313 ₄₅	0.734 ₂₂	0.093 ₆	0.431 ₃₁	0.379 ₂₇	0.791 ₂₁	0.086 ₅	0.440 ₁₆
	7.0	0.430 ₅₆	0.737 ₂₈	0.148 ₂₃	0.370 ₄₇	0.474 ₂₈	0.801 ₁₉	0.116 ₁₂	0.406 ₁₈

^a Subscripts give the statistical accuracies of the last decimal(s).

TABLE 9: Numerical Results of the Simulations for *n*-Heptane at 366 K and 450 K using the TraPPE-UA, OPLS-AA and TraPPE-EH Force Fields^a

	TraPPE-UA	OPLS-AA	TraPPE-EH	exp
<i>T</i> = 366 K				
<i>p</i>	0.126 ₁	0.098 ₄	0.087 ₅	0.08
ρ_{liq}	0.625 ₁	0.621 ₁	0.617 ₁	0.619
ρ_{vap}	0.0044 ₃	0.0034 ₁	0.0030 ₂	0.0028
ΔH_{vap}	29.7 ₂	33.9 ₁	32.4 ₁	32.2
<i>T</i> = 450 K				
<i>p</i>	0.781 ₅	0.943 ₆₅	0.677 ₂₀	0.637
ρ_{liq}	0.529 ₁	0.518 ₄	0.527 ₂	0.528
ρ_{vap}	0.026 ₂	0.033 ₄	0.022 ₁	0.021
ΔH_{vap}	23.2 ₃	24.4 ₃	25.6 ₂	25.12

^a Temperatures, (vapor) pressures, orthobaric densities, and heat of vaporization are given in units of K, MPa, g/mL, and kJ/mol, respectively. Experimental results are taken from ref 52. The subscripts give the statistical accuracy of the last decimal(s).

TABLE 10: Helium to *n*-Heptane Gibbs Free Energies of Transfer (in kJ/mol) and Specific Densities (in g/mL) at *T* = 298 K and *p* = 101.3 kPa Calculated Using the TraPPE-UA^{10,15} and TraPPE-EH Models^a

	exp	TraPPE-UA	run A	run B	run C
$\Delta G(\text{He})$	7.91	7.48 ₁₅	8.33 ₇	8.44 ₆	8.35 ₆
$\Delta G(\text{C}_5)$	-13.7	-12.75 ₂₄	-13.57 ₁₄		-13.76 ₂₀
$\Delta G(\text{C}_6)$	-16.6			-16.65 ₁₃	-16.66 ₂₅
$\Delta G(\text{C}_7)$	-19.5	-18.24 ₃₅	-19.70 ₁₀	-19.72 ₁₉	-19.70 ₁₉
ρ_{liq}		0.6845 ₉	0.6766 ₅	0.6756 ₅	0.6765 ₇
ρ_{vap}		0.00060 ₆	0.00041 ₁	0.00042 ₂	0.00040 ₂

^a The experimental data are taken from ref 61. Subscripts show the statistical accuracy of the last decimal(s).

energies of transfer calculated for the TraPPE-EH model are in good agreement with the experimental data,⁶¹ whereas the TraPPE-UA model has been found to underestimate the magnitude of the transfer free energies by approximately 1 kJ/mol (see Table 10).¹⁵ The accuracy of predictions of the free energies of transfer appears to be directly linked to the accuracy in calculations of pure-phase heats of vaporization, that is the TraPPE-UA model underestimates the heats of vaporization by 1 to 2 kJ/mol. Similarly, the TraPPE-EH force field gives a slightly too large heat of vaporization for the longer alkanes (octane and above), and also yields a free energy of transfer for *n*-heptane that is a bit too large in magnitude.

V. Conclusions

In this work, the TraPPE-EH force field for *n*-alkanes is developed and its performance is compared to that of the TraPPE-UA, OPLS-UA, and OPLS-AA models. Through this comparison, several open questions that were raised in the first paper of this series¹⁰ could be answered. First, the more realistic description of the shape of the *n*-alkanes afforded by the explicit-hydrogen representation allows us to find a model that is able to give satisfactory results for both liquid and vapor phases of single-component systems, that is critical temperatures and densities, normal boiling points, and accentric factors are much better reproduced by the TraPPE-EH force field than the TraPPE-UA model. Since both TraPPE force fields use Lennard-Jones potentials and neglect explicit many-body dispersive terms, we have to conclude that these have a smaller influence on the accuracies of the TraPPE force fields. Second, the TraPPE-EH force field that excels in the prediction of the single-component phase diagrams also outperforms the TraPPE-UA model for all multicomponent equilibria studied here. Future work involving mixtures with more polar fluids should answer the questions whether partial charges or induced polarizabilities

have to be added to the explicit-hydrogen representation to arrive at an alkane force field that is transferable over a wide range of physical conditions and chemical compositions.

Acknowledgment. We acknowledge many stimulating discussions with Doug Tobias, Mike Klein, Giacinto Scoles, and Mark Gordon. Financial support from the National Science Foundation (CTS-9813601), a Camille and Henry Dreyfus New Faculty Award, a McKnight/Land-Grant Fellowship, and a Sloan Research Fellowship is gratefully acknowledged. C.B. would like to thank the Graduate School, University of Minnesota, for the award of a Stanwood Johnston Memorial Fellowship. Part of the computer resources were provided by the Minnesota Supercomputing Institute.

References and Notes

- (1) Williams, D. E. *J. Chem. Phys.* **1967**, *47*, 4680.
- (2) Ryckaert, J. P.; Bellemans, A. *Faraday Discuss. Chem. Soc.* **1978**, *66*, 95.
- (3) Jorgensen, W. L.; Madura, J. D.; Swenson, C. J. *J. Am. Chem. Soc.* **1984**, *106*, 813.
- (4) Toxvaerd, S. *J. Chem. Phys.* **1990**, *93*, 4290.
- (5) Rodger, P. M.; Stone, A. J.; Tildesley, D. J. *Mol. Simul.* **1992**, *8*, 145.
- (6) Siepmann, J. I.; Karaborni, S.; Smit, B. *Nature* **1993**, *365*, 330.
- (7) Cornell, W. D.; Cieplak, P.; Bayly, C.; Gould, I. R.; Merz, K. M.; Ferguson, D. M.; Spellmeyer, D. C.; Fox, T.; Caldwell, J. W.; Kollman, P. A. *J. Am. Chem. Soc.* **1995**, *117*, 5179.
- (8) Jorgensen, W. L.; Maxwell, D. S.; Tirado-Rives, J. *J. Am. Chem. Soc.* **1996**, *118*, 11225.
- (9) Halgren, T. A. *J. Comp. Chem.* **1996**, *17*, 490, 520, 553, 616.
- (10) Martin, M. G.; Siepmann, J. I. *J. Phys. Chem. B* **1998**, *102*, 2569.
- (11) Martin, M. G.; Siepmann, J. I. *J. Phys. Chem. B* **1999**, *103*, 4508.
- (12) Errington, J. R.; Boulougouris, G. C.; Economou, I. G.; Panagiotopoulos, A. Z.; Theodorou, D. N. *J. Phys. Chem. B* **1998**, *102*, 8865.
- (13) Nath, S. K.; Escobedo, F. A.; de Pablo, J. J. *J. Chem. Phys.* **1998**, *108*, 9905.
- (14) Martin, M. G.; Siepmann, J. I. *J. Am. Chem. Soc.* **1997**, *119*, 8921. In these calculations a preliminary version of the TraPPE methyl group parameters ($\sigma = 3.77 \text{ \AA}$, $\epsilon/k_B = 98.1 \text{ K}$) was used in combination with the SKS methylene group parameters.
- (15) Martin, M. G.; Siepmann, J. I. *Theor. Chem. Acc.* **1998**, *99*, 347.
- (16) Kioupis, L. I.; Maginn, E. J. *Chem. Eng. J.* **1999**, in press.
- (17) Mondello, M.; Grest, G. S.; Webb, E. B.; Peczak, P. J. *Chem. Phys.* **1998**, *109*, 798.
- (18) Moller, M. A.; Tildesley, D. J.; Kim, K. S.; Quirke, N. *J. Chem. Phys.* **1991**, *94*, 8390.
- (19) Ryckaert, J. P.; McDonald, I. R.; Klein, M. L. *Mol. Phys.* **1989**, *67*, 957.
- (20) Chen, B.; Martin, M. G.; Siepmann, J. I. *J. Phys. Chem. B* **1998**, *102*, 2578.
- (21) van der Ploeg, P.; Berendsen, A. J. *Chem. Phys.* **1978**, *76*, 3271.
- (22) Scott, R. A.; Scheraga, H. A. *J. Chem. Phys.* **1966**, *44*, 3954.
- (23) McQuarrie, D. A. *Statistical Mechanics*; Harper and Row: New York, 1976; p 140.
- (24) Kollman, P. A. *Acc. Chem. Res.* **1996**, *29*, 461.
- (25) Tobias, D. J.; Tu, K.; Klein, M. L. *J. Chim. Phys. Phys. -Chim. Boil.* **1997**, *94*, 1482.
- (26) Smith, J. C.; Karplus, M. *J. Am. Chem. Soc.* **1992**, *114*, 801.
- (27) Lorentz, H. A. *Annalen Phys.* **1881**, *12*, 127.
- (28) Berthelot, D. C. R. *Hebd. Séances Acad. Sci.* **1898**, *126*, 1703.
- (29) Kaminski, G.; Jorgensen, W. L. *J. Phys. Chem.* **1996**, *100*, 18010.
- (30) MacKerrell, A. D. 1998, private communication.
- (31) Allinger, N. L. *Molecular Mechanics: Force Fields*; Burkert, U., Allinger, N. L., Eds.; ACS Monograph 77, American Chemical Society: Washington, DC, 1982.
- (32) Williams, D. E. *J. Chem. Phys.* **1965**, *43*, 4424.
- (33) Williams, D. E.; Starr, T. L. *Comput. Chem.* **1977**, *1*, 173.
- (34) Wertz, D. H.; Allinger, N. L. *Tetrahedron* **1974**, *30*, 1579.
- (35) Allinger, N. L. *J. Am. Chem. Soc.* **1977**, *99*, 8127.
- (36) Fitzwater, S.; Bartell, L. S. *J. Am. Chem. Soc.* **1976**, *98*, 5107.
- (37) Longuet-Higgins, H. C.; Salem, L. *Proc. Royal Soc. London* **1961**, *A259*, 433.
- (38) Salem, L. *J. Chem. Phys.* **1962**, *37*, 2100.

- (39) Amos, A. T.; Crispin, R. J. in *Theoretical Chemistry: Advances and Perspectives*; Eyring, H., Henderson, D., Eds.; Academic: New York, 1976; Vol. 2, p 2.
- (40) Kaplan, I. G. *Theory of Molecular Interactions*; Fraga, S., Klobukowski, M., Translation Eds.; Elsevier Science Publishers: Amsterdam, 1986.
- (41) Panagiotopoulos, A. Z. *Mol. Phys.* **1987**, *61*, 813.
- (42) Panagiotopoulos, A. Z.; Quirke, N.; Stapleton, M.; Tildesley, D. J. *Mol. Phys.* **1988**, *63*, 527.
- (43) Smit, B.; de Smedt, P.; Frenkel, D. *Mol. Phys.* **1989**, *68*, 931.
- (44) Siepmann, J. I. *Mol. Phys.* **1990**, *70*, 1145.
- (45) Siepmann, J. I.; Frenkel, D. *Mol. Phys.* **1992**, *75*, 59.
- (46) Frenkel, D.; Mooij, G. C. A. M.; Smit, B. *J. Phys.: Condens. Matter* **1992**, *4*, 3053.
- (47) de Pablo, J. J.; Laso, M.; Suter, U. W. *J. Chem. Phys.* **1992**, *96*, 2395.
- (48) Siepmann, J. I. *Computer Simulation of Biomolecular Systems: Theoretical and Experimental Applications*; van Gunsteren, W. F., Weiner, P. K., Wilkinson, A. J., Eds.; ESCOM Science: Leiden, 1993; Vol. 2, pp. 249–264.
- (49) Lal, M.; Spencer, D. J. *Chem. Soc., Faraday Trans 2* **1973**, *69*, 1502.
- (50) McQuarrie, D. A. *Statistical Mechanics*; Harper and Row: New York, 1976; p. 227.
- (51) Teja, A. S.; Lee, R. J.; Rosenthal, D.; Anselme, M. *Fluid Phase Equilib.* **1990**, *56*, 153.
- (52) Smith, B. D.; Srivastava, R. *Thermodynamic Data for Pure Compounds: Part A Hydrocarbons and Ketones*; Elsevier: Amsterdam, 1986.
- (53) Galassi, G.; Tildesley, D. J. *J. Mol. Sim.* **1994**, *13*, 11.
- (54) Chen, B.; Siepmann, J. I., unpublished results.
- (55) The other bonded (bending) and intramolecular Lennard–Jones energies are very similar for coexisting vapor and liquid phases for longer *n*-alkanes, e.g., the bending energy for the vapor phase for *n*-octane at 400 K is 9.93 kJ/mol versus 9.92 kJ/mol for the liquid phase calculated using the TraPPE-EH force field, and the intramolecular Lennard–Jones energy for the vapor phase is –2.49 kJ/mol versus –2.45 kJ/mol for the liquid phase.
- (56) Dymond, J. H.; Smith, E. B. *The Virial Coefficients of Pure Gases and Mixtures: A Critical Compilation*; Clarendon Press: Oxford, 1980.
- (57) Gehrig, M.; Lentz, H. *J. Chem. Thermodyn.* **1979**, *11*, 291.
- (58) Gehrig, M.; Lentz, H. *J. Chem. Thermodyn.* **1983**, *15*, 1159.
- (59) Toxvaerd, S. *J. Chem. Phys.* **1997**, *107*, 5197.
- (60) Knapp, H.; Döring, R.; Oellrich, L.; Prausnitz, J. M. *Vapor-Liquid Equilibria for Mixtures of Low Boiling Substances*; Schön and Wetzel: Frankfurt/Main, 1982.
- (61) Eiken, D. I. *Applicability of Theoretical and Semi-empirical Models for Predicting Infinite Dilution Coefficients*; Ph.D. Thesis, University of Minnesota, 1993.
- (62) Daubert, T. E.; Danner, R. P. *Physical and Thermodynamic Properties of Pure Chemicals: Compilation 1*; Hemisphere Pub. Corp.: New York, 1989.